AIAA JOURNAL
Vol. 36, No. 6, June 1998

Emission and Holographic Interferometry Measurements in a Superorbital Expansion Tube

Timothy J. McIntyre,* Alexis I. Bishop,† Amberyn M. Thomas,† Margaret J. Wegener,†
and Halina Rubinsztein-Dunlop‡
University of Queensland, Brisbane, Queensland 4072, Australia

Free-piston-driven expansion tubes are capable of generating flow conditions over a wide range of enthalpies ranging from orbital up to superorbital velocities. Initial optical measurements aimed at investigating the flow in such a facility are presented. Emission studies were used to identify impurities in the flow and to investigate spectral regions that are accessible by optical techniques. At moderate enthalpies, it was found that significant radiation resulted from metallic contaminants. At high enthalpies, the spectrum consisted of a number of atomic lines together with a broadband background component indicative of the presence of electrons. The presence of this radiation may limit the applicability of optical techniques that require spectral regions free from the influence of atomic transitions or background radiation. Emission spectroscopy (through Stark broadened hydrogen lines) and two-wavelength holographic interferometry were used to measure the electron number density behind a bow shock on a blunt body at conditions where significant ionization was observed. They yielded average concentrations of $(3 \pm 1) \times 10^{17}\,\mathrm{cm}^{-3}$ from the emission measurements and $(3.8 \pm 0.6) \times 10^{17}\,\mathrm{cm}^{-3}$ from the interferometry.

Nomenclature

A = atomic species (here N or O)
A^+ = singly ionized species
C = constant
e^- = electron
G = Gladstone–Dale coefficient
K = constant
l = path length for the interferometry
M = collision partner
m = atomic mass
N_e = electron number density
p = fringe shift
r = ratio of the Gladstone–Dale coefficient for the ion to that for the atom
λ = wavelength
ρ = total density

Subscripts

A = atomic species in the flow
N = nitrogen atoms
O = oxygen atoms
1 = value at wavelength 1
2 = value at wavelength 2
∞ = conditions in the freestream

Introduction

THE development of superorbital expansion tubes has led to the generation of a new flow regime in which aerodynamic testing can be performed.[1] Airflows with enthalpies above 80 MJ/kg and velocities around 11 km/s have been obtained, simulating the re-entry conditions experienced by vehicles on superorbital missions. For measurement techniques, these facilities provide new challenges, including short test times, significant levels of ionization, and intense flow luminosity.

A number of advanced optical diagnostic techniques have been developed and applied to testing in high-enthalpy, free-piston-driven facilities.[2] Interferometry has provided flow visualization and density distributions,[3,4] planar laser-induced fluorescence[5] (PLIF) and coherent anti-Stokes Raman scattering[6] (CARS) have been used to measure temperature, and laser-enhanced ionization has been utilized to measure velocity.[7] The study of the applicability of such techniques to the extreme conditions experienced in superorbital expansion tubes was one of the aims of this work. A spectrally resolved study of the flow luminosity was performed at moderate and high enthalpies to investigate the species present and to determine the wavelengths at which optical measurements could be performed. Previous measurements in high-enthalpy facilities[8,9] have shown the presence of metallic components, particularly iron, in the flow. The current investigation was aimed at identifying which radiating species are present both at moderate enthalpies (similar to the enthalpies studied previously in shock tunnels) and at the high enthalpies uniquely generated here.

The second aim of the study was to quantify the presence of electrons behind a bow shock on a blunt body at the high-enthalpy condition. This was possible through the use of two methods. Stark broadening data for atomic hydrogen lines that were observed in the emission spectra allowed the estimation of the average electron concentration in the bow shock region. To provide more accurate, spatially resolved measurements, two-wavelength holographic interferometry was implemented. A single holographic plate was used to record holograms at two well-separated wavelengths, which yielded sufficient data for the simultaneous evaluation of electron density and total density.[10] These measurements also enabled the visualization of the flowfield, including the bow shock shape.

Facility

All experiments were performed in the X1 superorbital expansion tube at the University of Queensland.[1] The layout for the tunnel is shown in Fig. 1. A free-piston driver was used to generate a high-temperature, high-sound-speed driver gas. For the highest enthalpy condition, a secondary driver was also used. Upon rupture of the primary and secondary diaphragms, a strong shock was generated, which passed through the test gas (bottled dry air) and then into the accelerator tube. The test gas was processed by an unsteady expansion, accelerating it to the freestream conditions at which it exited the tube and passed over the model of interest. For the studies presented here, two experimental conditions were investigated. First, a moderate enthalpy condition (14 MJ/kg, denoted condition A) was utilized for comparison with previous work in shock tunnels that are capable of generating similar conditions. Second, a high-enthalpy condition (93 MJ/kg, denoted condition B) was investigated to study

Presented as Paper 97-0775 at the AIAA 35th Aerospace Sciences Meeting, Reno, NV, Jan. 6–9, 1997; received Feb. 28, 1997; revision received Sept. 25, 1997; accepted for publication Jan. 26, 1998.

*Research Fellow, Department of Physics. Member AIAA.
†Postgraduate Student, Department of Physics.
‡Associate Professor, Department of Physics.

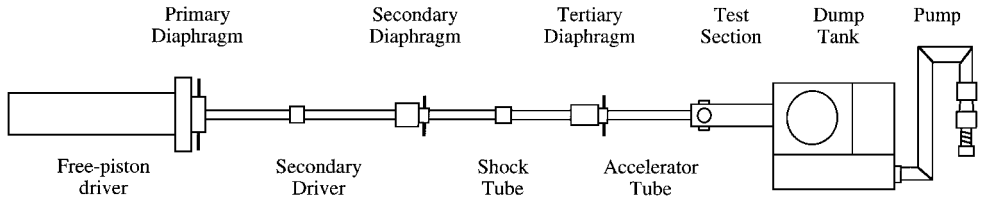

Fig. 1 Schematic diagram of the X1 superorbital expansion tube facility.

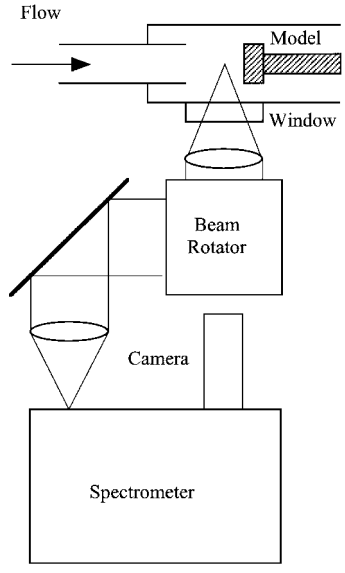

Fig. 2 Plan view of the arrangement for emission measurements in the X1 superorbital expansion tube.

Table 1 Calculated conditions in the freestream and behind a bow shock in the X1 superorbital expansion tube (assuming chemical and thermal equilibrium)

	A, Moderate enthalpy		B, High enthalpy	
Parameter	Freestream	Bow shock	Freestream	Bow shock
Pressure, kPa	35	580	29	850
Temperature, K	3,270	6,400	7,160	15,900
Density, kg/m^3	0.035	0.25	0.0079	0.072
Enthalpy, MJ/kg	14	14	93	93
Velocity, km/s	4.27	0.6	10.8	1.2
Mach number	3.7	0.3	4.7	0.29
Dissociation fraction N_2	——	0.11	0.78	1.0
Dissociation fraction O_2	0.43	1.0	1.0	1.0
%NO	4.1	1.4	0.1	——
Ionization fraction N	——	——	——	0.31
Ionization fraction O	——	——	——	0.21
Electron concentration (cm^{-3})	——	——	——	8.8×10^{17}

superorbital flows. The operating conditions are given in Table 1. The quoted values are calculated, presuming chemical and thermal equilibrium throughout the flow, based on measurements of fill pressures and shock speeds. The test time obtained in the tunnel ranged from about 100 μs for the moderate-enthalpy condition down to about 30 μs for the high-enthalpy condition. This tunnel is a forerunner to several larger facilities, one currently in a calibration phase (X2) and the other under construction (X3).[11]

For all measurements, the flow over a 20-mm-diam cylinder of width 25 mm was investigated. The model was placed immediately at the exit of the 38-mm-diam expansion tube in a specially constructed test section with optical access.

Method

Emission

Spectrally resolved emission studies were performed to examine species in the flow and to investigate wavelength regions free from interferences from luminosity where optical measurements may be performed. The experimental arrangement for the measurements is shown in Fig. 2. The flow in front of a cylinder was imaged onto the entrance slit of an imaging spectrometer (SPEX 270M, 270 mm length, 600 lines/mm grating) so that spatial resolution was obtained along the stagnation streamline before and after the bow shock. Fused silica windows and optics were used, allowing spectral measurements down to 200 nm. The spectrally and spatially resolved output was imaged onto a fast-gated, intensified, charge-coupled device camera (Princeton Instruments) with a uv-enhanced photocathode. The resolution of the spectrometer and size of the detector allowed for a 70-nm-wide spectrum to be recorded in each shot. A complete spectrum ranging from 200 nm up to 600 nm was recorded in successive shots by stepping the spectrometer 50 nm after each shot. The camera gate and spectrometer entrance slit were selected for each enthalpy condition to ensure that signal levels did not saturate the detector. Focusing and sensitivity of the optical system varied somewhat with wavelength. No effort was made to correct for these changes.

The presence of atomic hydrogen lines in the high-enthalpy case allowed for the measurement of electron concentrations through the process of Stark broadening.[12] The electric field due to the electrons causes splitting of the hydrogen energy levels via the linear Stark effect. The resulting broadening of the emission lines thus provides a sensitive way of measuring the electron concentration. For hydrogen lines, the broadening is described by the quasistatic model, which gives a linewidth $\Delta\lambda$ of[13]

$$\Delta\lambda = C N_e^{\frac{2}{3}} \tag{1}$$

where N_e is the electron concentration and C has only a weak dependence on electron number density and temperature. Various sets of tables exist for determining the electron concentration from the line shape. A set of computed tables[14] is used in this case that provides broadening data over temperatures ranging from 2500 to 160,000 K and electron concentrations of 10^{10}–10^{18} cm^{-3}. The complete line shape is calculated for given values of temperature and electron concentration and then compared with the experimental measurements.

Holographic Interferometry

Holographic interferometry was used for flow visualization and to obtain quantitative information on the flow density and electron concentration. The layout of the system is shown in Fig. 3. The frequency-doubled and frequency-tripled outputs of an injection-seeded Nd:YAG laser (Continuum NY81) were used, yielding a laser beam output containing wavelengths of 532 and 355 nm. The intensities of these wavelengths were varied independently to give optimal holographic recording. The beam was divided into two parts (each containing both wavelengths), with one beam being expanded and passed through the test section while the second beam was passed around the tunnel by the use of periscopes. The beams were combined on a Kodak 120-01 holographic plate, forming an image plane hologram of the model in the test section. An aperture was positioned in the test section beam to eliminate flow luminosity. Holograms at the two wavelengths were simultaneously recorded on a single holographic plate for, first, the no-flow situation and, second, the with-flow situation. Upon illuminating the processed plate with a helium–neon laser or sodium lamp, the reconstructed beams recorded with the lower wavelength were diffracted at a larger angle than those from the higher wavelength, and thus the two interferograms were spatially separated and could be observed and recorded independently.

The analysis of the images proceeded as follows. The fringe shift referenced to the freestream was measured at each point along the

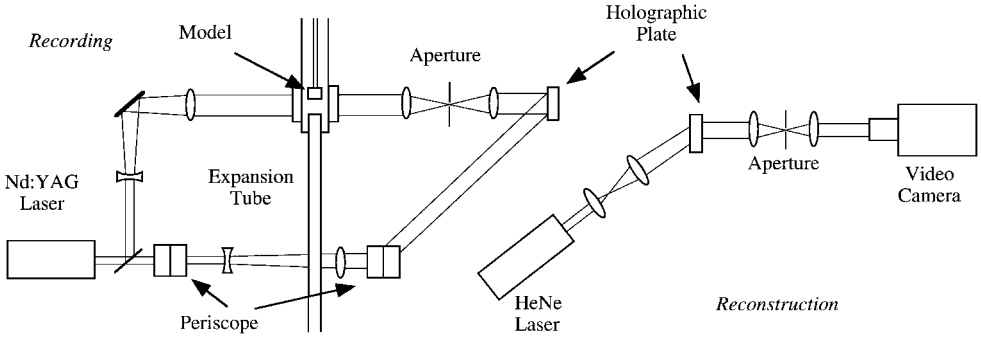

Fig. 3 Experimental arrangement for holographic interferometry in the X1 superorbital expansion tube.

stagnation streamline, providing one set of values for the wavelength of 355 nm and one set for 532 nm. This fringe shift can be described by the equation[10]

$$\Delta p_\lambda = \frac{G_{A\lambda}\Delta\rho_A l}{\lambda} + \frac{G_{A^+\lambda}\Delta\rho_{A^+} l}{\lambda} - K\Delta N_e \lambda l \qquad (2)$$

where the first term describes the effect due to the neutral species A, the second term is the effect due to ionized atoms A^+, and the last term is the (negative) fringe shift due to the electrons. Because we are considering reactions of the type

$$A + M \Leftrightarrow A^+ + e^- + M \qquad (3)$$

the number of ions is equal to the number of electrons. Equation (2) can, therefore, be reduced to an equation with two unknowns: the total density of the flow and the electron number density. The two sets of measurements (355 and 532 nm) provide two independent equations of the type given by Eq. (2), which can be solved simultaneously to obtain the quantities

$$\rho = \rho_\infty + \frac{(p_1 - p_{1\infty})\lambda_1 K_2 - (p_2 - p_{2\infty})\lambda_2 K_1}{(G_1 K_2 - G_2 K_1) l}$$

$$N_e = N_{e\infty} + \frac{(p_1 - p_{1\infty})\lambda_1 G_2 - (p_2 - p_{2\infty})\lambda_2 G_1}{(G_1 K_2 - G_2 K_1) l} \qquad (4)$$

For a single species A, the constant K_i can be written

$$K_i = K\lambda_i^2 + G_{Ai} m_A (1 - r_A) \qquad (5)$$

where the subscript i refers to values of the parameter at the wavelength λ_i.

The measurements presented here used a test gas of air, and thus application of the given equations requires some extra assumptions. Table 1 shows that, at the high-enthalpy condition, the freestream consists mostly of atomic rather than molecular species, whereas behind the bow shock only atoms and ions are present. To a good approximation, the gas can be considered as consisting of only atomic oxygen and atomic nitrogen together with ionized species. Contributions to the fringe shift from both of these species must, thus, be considered. This can be achieved by defining a Gladstone–Dale coefficient for the neutral species, which is effectively a linear combination of the constituent coefficients weighted by the proportions of the respective species (80% nitrogen, 20% oxygen):

$$G_i = \frac{0.8 G_{Ni} m_N}{m_{air}} + \frac{0.2 G_{Oi} m_O}{m_{air}} \qquad (6)$$

The Gladstone–Dale coefficient for the ions, as given by the parameter r_A, is more difficult to quantify. Given the lack of experimental measurements of this quantity, it is here assumed that the value of the Gladstone–Dale coefficient for the ion is equal to the value for the atom. The error introduced by this assumption has only a minimal effect on the measured electron number density.[10]

Results

Emission

Sample images of the spectra obtained at moderate and high enthalpies are shown in Fig. 4. These images show a wavelength region of some 70 nm along a spatial axis aligned with the stagnation streamline. The locations of the shock and model are indicated. These are particularly distinct at the higher-wavelength end of the spectra. However, toward the uv, the focus is not as sharp due to the change in the power of the optical elements with wavelength. The intensity of light falling on the detector is controlled by the size of the spectrometer entrance slit and the duration for which the camera is exposed. For the moderate-enthalpy condition, a spectrometer slit width of 100 μm and a camera gate duration of 500 ns were used, whereas for the high-enthalpy condition these were 10 μm and 100 ns, respectively. Thus, the spectra for the high-enthalpy case were approximately 50 times stronger than in the moderate-enthalpy case. The size of the entrance slit together with the pixel spacing of the camera influences the resolution of the detection system. For the moderate-enthalpy case, the resolution at the exit of the spectrometer was calculated to be 0.6 nm, whereas for the high-enthalpy case, the resolution was 0.2 nm.

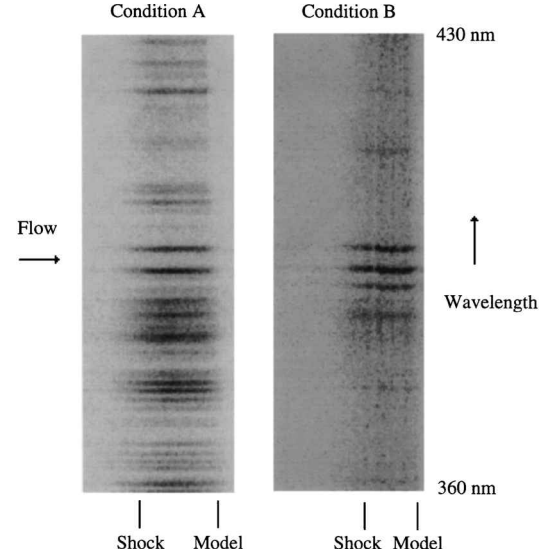

Fig. 4 Emission images; intensities for the high-enthalpy condition B are approximately 50 times those for the moderate-enthalpy condition A (see conditions in Table 1).

The spectra show a very small signal ahead of the shock front (due to the temperature of the freestream) followed by a dramatic increase as the gas was heated and compressed through the shock. There was little variation in the intensity or spectral distribution of the light along the stagnation streamline between the shock and the body. To obtain spectra from these images, the entire region between the shock front and the body was averaged in the spatial direction and plotted as a function of wavelength. The resulting spectra from the images shown in Fig. 4 are given in Fig. 5. The absolute value for the wavelength was determined from the spectrometer setting, which was calibrated, where possible, by the use of known spectral lines from mercury and sodium lamps. Prominent lines in the spectra from species expected to be in the flow (such as iron and sodium) were used to cross check the calibration.

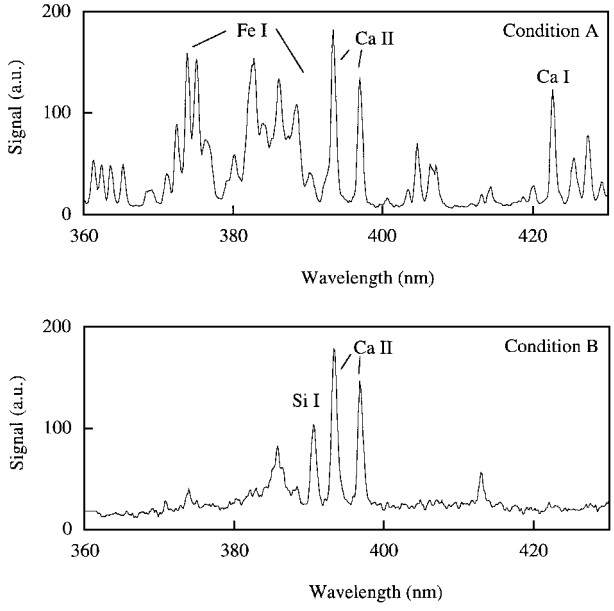

Fig. 5 Recorded spectra behind the bow shock on a cylinder corresponding to the images shown in Fig. 4; intensities for the high-enthalpy condition B are approximately 50 times those for the moderate-enthalpy condition A.

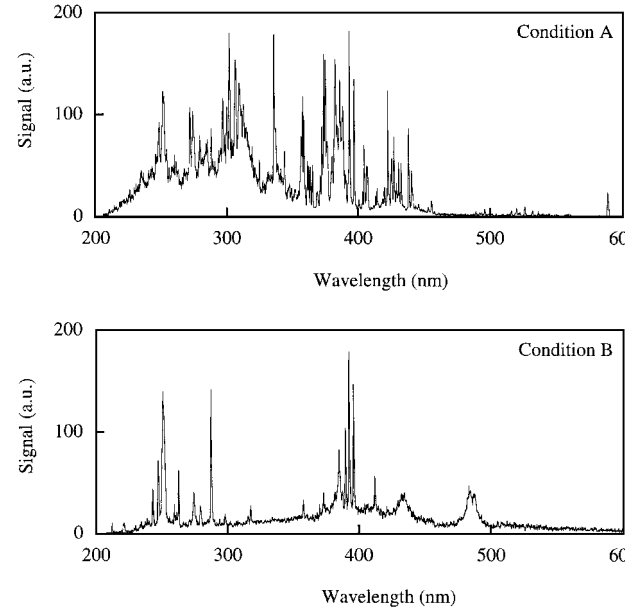

Fig. 6 Recorded spectra behind the bow shock on a cylinder for a wavelength range of 200–600 nm; intensities for the high-enthalpy condition B are approximately 50 times those for the moderate-enthalpy condition A.

For the moderate-enthalpy case, the majority of the observed lines in Fig. 5 can be attributed to the metallic contaminant iron from the steel tube and/or diaphragm. As well, bright lines due to calcium ions were observed, and contributions at other wavelengths can be attributed to silicon, sodium, and other trace metallic components. The presence of these contaminants was most likely due to their entrainment into the flow as the hot test gas passed along the tube.

The spectral distribution in the high-enthalpy case shows, in contrast, far fewer spectral lines in the same wavelength range. Whereas the calcium ion lines persist, the iron lines are no longer identifiable, showing that iron is not a significant contributor to the total radiation. The remaining spectral line in Fig. 5 is thought to be due to silicon (also observed at other wavelengths), which was probably present due to either the use of a silicon oil diffusion pump for this condition or the use of silicon vacuum grease in the facility. The background radiation is now comparatively stronger than before, obscuring any other spectral lines that may be present. The other spectral features evident in Fig. 5 have not been conclusively identified.

Complete spectra for both conditions over a wavelength range from 200 to 600 nm are given in Fig. 6. These were obtained by overlapping eight spectra of the type given in Fig. 5 for each enthalpy. No attempt has been made to convert these spectra to absolute intensity measurements. Also note that the spectral response of the spectrometer and photodetector are not constant across this wavelength range, so that intensity levels over wide wavelength ranges should not be compared.

The spectra for the moderate-enthalpy case show a large number of narrow lines, which can be attributed to atomic species, as well as broader features, which may be collections of closely spaced atomic lines or, alternatively, molecular bands (possibly OH and NO). In general, the spectra are very similar to those reported previously for a shock tunnel,[8,9] with the majority of the radiation lying in the wavelength range between 200 and 450 nm. No evidence of molecular nitrogen or oxygen bands was found. The transitions in these species are much weaker than in the metallic species, and thus emission is likely to be below the current detection limit.

For the high-enthalpy case, the absence of a large number of spectral lines noted in Fig. 5 is continued over the wider spectral range. The two major lines between 200 and 300 nm can be attributed to silicon. Other lines have not been conclusively identified. Atomic nitrogen and oxygen have spectral features throughout the visible spectrum. However, no lines were identified from these species. The expected intensities of these lines would have been relatively low so that they were probably obscured by the intensity of the background radiation.

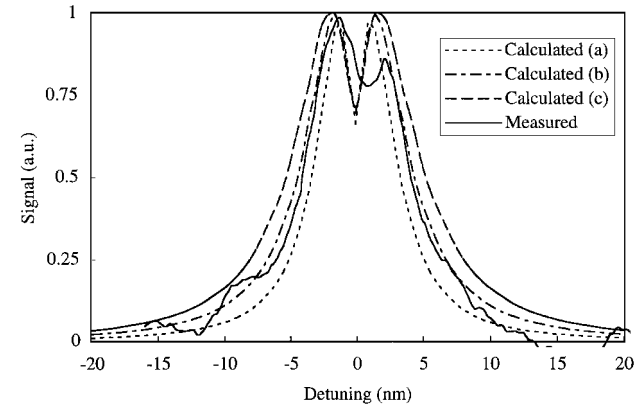

Fig. 7 Experimental and calculated profiles for the Stark broadened H–β emission line at 486.1 nm; solid line is the experimentally measured profile, and dashed lines show predicted profiles for values of the electron number density of a) 2×10^{17} cm^{-3}, b) 3×10^{17} cm^{-3}, and c) 4×10^{17} cm^{-3}.

There are several possible sources for this background radiation. The most likely contributors are from ion–electron recombinations and/or bremsstrahlung. This is supported by the uniform nature of the radiation across the visible spectrum. Weaker atomic lines may also contribute to this signal.

The two broad features shown in Fig. 6 at the high-enthalpy condition can be identified as the H–β (486.1-nm) and H–γ (434.1-nm) lines from the Balmer series of atomic hydrogen. (The H–α line at 656.3 nm is outside the spectral region investigated.) This identification is based on the spectral position as well as shape of the spectral lines. These are much broader than other lines because hydrogen experiences the linear Stark effect, whereas other species exhibit only the weaker quadratic Stark effect. The source of the hydrogen in the flow is uncertain but is most likely due to the presence of water on the walls of the tunnel that is not completely removed during the evacuation process. To quantify the electron density causing the broadening, the profile of the H–β line was extracted from the background and compared with numerical simulations of the linewidth using the electron number density as a free parameter to provide the best fit. These results are shown in Fig. 7. The solid line is the experimentally measured profile (obtained by averaging across the whole region between the bow shock and the body), whereas the dashed lines show calculated linewidths for different electron number densities. As input to the code, a flow temperature of 15,000 K,

taken from the estimated equilibrium conditions, was used. For the H–β line, the influence of temperature is very minor, with predicted full widths changing by less than 1 nm over a temperature range from 10,000 to 20,000 K. The fit shown in Fig. 7 for an electron concentration of 3×10^{17} cm^{-3} is good, in general, with the major discrepancy being at the peak on the higher-wavelength side of the line. This is thought to result from the low signal levels recorded. The curves allowed us to estimate the average electron density between the shock and the body to be $(3 \pm 1) \times 10^{17}$ cm^{-3}. This is below the estimated equilibrium value of 8.8×10^{17} cm^{-3} given in Table 1. Further discussion concerning electron concentration is presented in the Holographic Interferometry section.

The significance of the spectral distributions of the emission is twofold. First, from the point of view of the optical measurements, it is clear, particularly for the high-enthalpy condition, that substantial filtering of the radiation will be necessary. A concern for holographic interferometry is the presence of strong spectral lines likely to perturb the background refractive index of the gas. No such features for either condition were observed at the wavelength of 532 nm, which is currently used for holographic interferometry on this facility. Second, for condition B, there were no spectral influences at the wavelength of 355 nm, which (together with 532 nm) is used for two-wavelength holographic interferometry. The majority of the background radiation can be removed by the use of interference filters and aperturing for interferometric techniques. However, careful wavelength selection will be required for spectroscopic techniques. Methods such as PLIF, degenerate four-wave mixing, CARS, and near-resonant holographic interferometry all require selected wavelengths that must be free from interference from other species in the flow. As well, the output signal for each method must be detected without contributions from background signals that lead to low signal-to-noise measurements. The selection of these wavelengths must be made so as to avoid interferences from contaminant species.

The spectral distribution is also of significance when considering heat transfer. For the high-enthalpy condition, velocities are such that radiative heat transfer may form a significant proportion of the total heat transfer.[15] From the measurements performed here in the visible and uv regions of the spectrum, it is seen that a proportion of the radiation comes from contaminant species and so will not be truly representative of the flow regime. Comparisons of heat transfer with numerical simulations[15] may need to take such contributions into consideration. Further investigation is required to determine whether this is the case across the whole of the spectrum over which radiative heat transfer is significant.

Holographic Interferometry

In a previous study, we investigated an airflow with a velocity of 11 km/s over a range of wedges and measured the angles of the attached shocks, which compared favorably with calculations.[3] The flow over a cylinder was also studied, and it was observed that significant relaxation occurred. This was evident as a negative fringe shift behind the bow shock, indicating the liberation of electrons as collisions within the shock-heated gas began to ionize the flow. The process is initiated by atom–atom collisions but is accelerated when a significant electron population is generated. These electrons have a higher mobility and a higher collisional cross section, which leads to an avalanche effect. Their presence means that it is not possible to obtain quantitative measurements on density distribution from a single interferogram.

Quantitative measurements can be made when interferograms at two sufficiently separated wavelengths are recorded. This is possible because the fringe shift due to electrons becomes larger for longer wavelengths, whereas that due to heavy particles decreases [see Eq. (2)]. Sample interferograms recorded using two-wavelength holographic interferometry are shown in Fig. 8. These images were recorded simultaneously in the flow: Fig. 8a using a wavelength of 355 nm and Fig. 8b with a wavelength of 532 nm. In each case, some influence from flow luminosity can be observed behind the bow shock, where fringe visibility decreases. Toward the sides of the body, fringe shifts across the shock show a small positive jump as the total density increases. This is followed by a negative shift (more pronounced near the center of the image), indicating the liberation of electrons. This occurs almost immediately behind the bow shock on the stagnation streamline, indicating that the onset time for generation of electrons is very short in this flow.

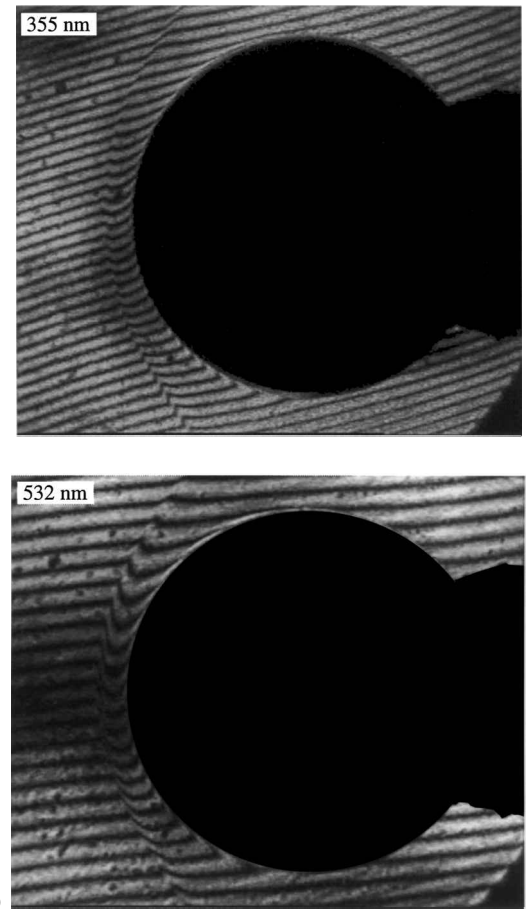

Fig. 8 Holographic interferogram of the flow over a cylinder at the high-enthalpy condition B; flow is from left to right; positive fringe shift is upward; images were recorded with laser wavelengths of 355 and 532 nm.

To obtain quantitative measurements, fringe shifts along the stagnation streamline were measured from each interferogram, and the total density and electron concentration were determined using the method described. These results are shown in Fig. 9, where each point corresponds to a measurement of the fringe shift, and the estimated uncertainty in the experiment is shown. The calculated freestream density (see Table 1) was used in the determination of the total density, whereas the freestream electron concentration was presumed to be zero. The total density increases instantaneously across the shock and continues to increase as the gas relaxes. Ignoring the molecular component of the freestream, the frozen density jump across the shock front would be expected to be a factor of six. The measured jump is smaller than this, indicating that edge effects in the flow over the cylinder may be significant, reducing the true path length of the interferometry in the vicinity of the shock. Nearer the body, an almost constant density is approached, which agrees well with the calculated equilibrium value for a blunt body quoted in Table 1. The electron concentration also increases behind the shock and reaches a maximum value of $(4.6 \pm 0.5) \times 10^{17}$ cm^{-3} about halfway between the body and the shock. Beyond this point the concentration decreases. The average value throughout the bow shock region is $(3.8 \pm 0.6) \times 10^{17}$ cm^{-3}, which is closer to the value of $(3 \pm 1) \times 10^{17}$ cm^{-3} measured from the hydrogen line broadening than the estimated equilibrium concentration of 8.8×10^{17} cm^{-3}.

There are two possible explanations for why the measured value is significantly lower than the calculated value. First, the determination of the freestream conditions relies on upstream measurements in the flow together with a calculation that assumes chemical and thermal equilibrium throughout. This assumption is probably not valid, especially through the expansion stage where the gas is accelerated. More accurate simulations need to be developed. Second,

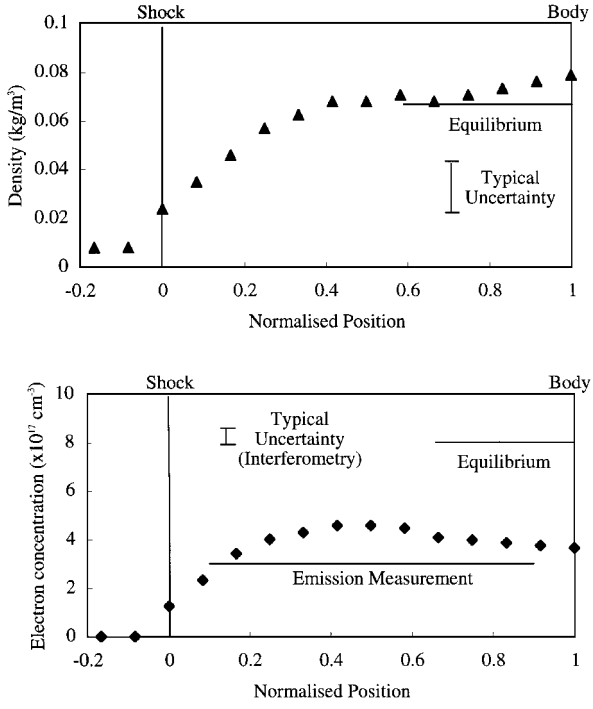

Fig. 9 Total density and electron concentration along the stagnation streamline for the flow over a cylinder measured from the images in Fig. 8; shock standoff distance, measured from Fig. 8, is (1.7 ± 0.2) mm.

due to the extremely high temperatures, a significant amount of heat is lost in the form of radiation. In this case, temperatures lower than that predicted by the code would be obtained in the stagnation region, leading to lower equilibrium electron concentrations in accordance with the results obtained here.

Conclusions

Emission studies performed in a superorbital facility have established the presence of a number of strongly radiating impurities in the flow. These impurities are most likely mixed into the test gas as it passes along the tube and, when heated in the shock layer, radiate over a range of wavelengths in the visible and uv parts of the spectrum. At high enthalpy, far fewer spectral lines with a larger relative continuum background were observed. Optical techniques will require efficient spectral filtering and/or aperturing to be applicable at these conditions. Broadened atomic hydrogen lines were observed from which the electron concentration between the shock and the body was deduced to be $(3 \pm 1) \times 10^{17}$ cm^{-3}.

A two-wavelength holographic interferometry technique has been applied to study the total density and electron density along the stagnation streamline. Total density measurements agreed well with equilibrium predictions. Electron density measurements compared well with the values obtained from the emission studies but were lower than those calculated using equilibrium assumptions.

Acknowledgments

This work was financially supported by the Australian Research Council and the University of Queensland. The authors would like to acknowledge the assistance of Richard Morgan, Ray Stalker, and Mark Sutcliffe in obtaining suitable conditions in the tunnel. Workshop assistance from the Departments of Physics and Mechanical Engineering is also acknowledged.

References

[1]Neely, A. J., and Morgan, R. G., "The Superorbital Expansion Tube Concept, Experiment and Analysis," *Aeronautical Journal*, Vol. 98, No. 973, 1994, pp. 97–105.

[2]Simmons, J. M., "Measurement Techniques in High Enthalpy Hypersonic Facilities," *Experimental Heat Transfer, Fluid Mechanics and Thermodynamics*, edited by M. D. Kelleher, Elsevier, New York, 1993, pp. 43–60.

[3]Wegener, M. J., McIntyre, T. J., Rubinsztein-Dunlop, H., Bishop, A. I., Stalker, R., and Morgan, R. G., "Visualization and Analysis of Bow Shocks in a Superorbital Expansion Tube," *AIAA Journal*, Vol. 34, No. 10, 1996, pp. 2200–2202.

[4]Boyce, R. R., Morton, J. W., Houwing, A. F. P., Mundt, C., and Bone, D. J., "Computational Fluid Dynamics Validation Using Multiple Interferometric Views of a Hypersonic Flowfield," *Journal of Spacecraft and Rockets*, Vol. 33, No. 3, 1996, pp. 319–325.

[5]Palma, P. C., McIntyre, T. J., and Houwing, A. F. P., "PLIF Thermometry in Shock Tunnel Flows Using a Raman-Shifted Tunable Excimer Laser," *Shock Waves* (to be published).

[6]Boyce, R. R., Pulford, D. R. N., Houwing, A. F. P., and Mundt, C., "Rotational and Vibrational Temperature Measurements Using CARS in a Hypervelocity Shock Layer Flow and Comparisons with CFD Calculations," *Shock Waves*, Vol. 6, No. 1, 1996, pp. 41–51.

[7]Littleton, B. N., Bishop, A. I., McIntyre, T. J., Barker, P. F., and Rubinsztein-Dunlop, H., "Flow Tagging Velocimetry in a Superorbital Expansion Tube," *Proceedings of the 21st International Symposium on Shock Waves*, edited by A. F. P. Houwing, Panther Publishing and Printing, Australia, 1998 (Paper 4491).

[8]Palma, P. C., Houwing, A. F. P., and Sandeman, R. J., "Absolute Intensity Measurements of Impurity Emissions in a Shock Tunnel and Their Consequences for Laser-Induced Fluorescence Measurements," *Shock Waves*, Vol. 3, No. 1, 1993, pp. 49–53.

[9]Beck, W. H., Müller, M., and Wollenhaupt, M., "Application of Spectroscopic Diagnostic Techniques to Studies on HEG: Preparatory LIF Work and Emission Spectroscopy Results," *15th International Congress on Instrumentation in Aerospace Simulation Facilities*, Institut Franco–Allemand de Recherche, Saint-Louis, France, 1993.

[10]McIntyre, T. J., Wegener, M. J., Bishop, A. I., and Rubinsztein-Dunlop, H., "Simultaneous Two-Wavelength Holographic Interferometry in a Superorbital Expansion Tube Facility," *Applied Optics*, Vol. 36, 1997, pp. 8128–8134.

[11]Morgan, R., "A Review of the Use of Expansion Tubes for Creating Superorbital Flows," AIAA Paper 97-0279, Jan. 1997.

[12]Griem, H. R., *Spectral Line Broadening by Plasmas*, Academic, New York, 1974.

[13]Thorne, A. P., *Spectrophysics*, Chapman and Hall, London, 1988, p. 376.

[14]Lemke, M., "Extended VCS Stark Broadening Tables for Hydrogen—Lyman to Brackett Series," *Astronomy and Astrophysics Supplement Series*, Vol. 122, 1997, pp. 285–292.

[15]Rochelle, W. C., An, M. Y., Tam, L. T., Williams, S. D., and Curry, D. M., "High Energy Entry Heating Study for Lunar/Mars Aerocapturing Vehicles," AIAA Paper 94-2002, June 1994.

G. Laufer
Associate Editor